Longitudinal modulation of the O/N_2 column density retrieved from TIMED/GUVI measurement

Maosheng He,[1,2] Libo Liu,[1] Weixing Wan,[1] Jiuhou Lei,[3] and Biqiang Zhao[1]

Received 12 August 2010; accepted 17 September 2010; published 27 October 2010.

[1] The longitudinal variation of thermospheric O/N_2 column density ratio is studied, based on the TIMED/GUVI measurements collected during 2002-2007. In October, a four-peaked longitudinal fluctuation in O/N_2 is found. The wavenumber-4 fluctuation in equatorial O/N_2 is generally stronger at lower solar activity, and maximizes in the morning of boreal summer and autumn. In boreal winter, the wavenumber-4 component gives way to the wavenumber-3. Such seasonal variation and solar activity dependence are consistent with those of the diurnal eastward-propagating mode with wavenumber-3, but the local time dependence is not. The daytime wavenumber-4 pattern in O/N_2 does not shift eastward in local time as expected if it is directly connected to the DE3. No definite explanation is found for this structure, but a consideration of various mechanisms suggests that the vertical wind effect may be the most potential candidate. **Citation:** He, M., L. Liu, W. Wan, J. Lei, and B. Zhao (2010), Longitudinal modulation of the O/N_2 column density retrieved from TIMED/GUVI measurement, *Geophys. Res. Lett.*, *37*, L20108, doi:10.1029/2010GL045105.

1. Introduction

[2] The diurnal cycle of solar insolation excites atmospheric tides characterized as large-scale waves in temperature, density and winds with periods that are harmonics of a solar day [e.g., *Hagan and Forbes*, 2002; *Forbes et al.*, 2008, and references therein]. The non-sunsynchronous tidal components are termed as nonmigrating tides. Among the nonmigrating tides, the diurnal eastward-propagating mode with wavenumber-3 (DE3 for short) is the most dynamical component in the thermosphere during most of the year [e.g., *Hagan and Forbes*, 2002]. The DE3 mode is suggested to be induced by latent heat release in the troposphere [*Hagan and Forbes*, 2002]. When propagating upward, the DE3 mode grows exponentially. Finally, the tide dissipates and deposits momentum and energy directly into the mesosphere, lower thermosphere, and possibly the upper thermosphere [*Hagan et al.*, 2009]. There is a general agreement that the DE3 mode imposes remarkable signatures in the ionosphere, thermosphere and mesosphere. When the DE3 tide is observed in a fixed local time frame such as from the slowly precessing satellite, four zonal wave patterns (i.e., wavenumber-4 structure, or simply WN4) would be recorded diurnally, due to the blueshift of Doppler Effect [also cf. *Oberheide et al.*, 2003].

[3] The WN4 structure was first reported in the airglow brightness of 135.6 nm [*England et al.*, 2006; *Immel et al.*, 2006]. Subsequently, the structure was observed in various ionospheric and thermospheric properties [e.g., *Häusler et al.*, 2007; *Wan et al.*, 2008; *Ren et al.*, 2008; *Liu et al.*, 2009a, 2009b; *Forbes et al.*, 2009; *Huang et al.*, 2010]. *Oberheide and Forbes* [2008a] reported a WN4 signature in thermospheric nitric oxide density based on SNOE observations, and they speculated that the longitudinal fluctuation induced by nonmigrating tides may also exist in other thermospheric compositions and airglow emissions, such as atomic oxygen densities and O/N_2 ratio.

[4] In the ionospheric F-region, electron production is primarily due to the photoionization of atomic oxygen and the loss rate is proportional to the density of molecular compositions (primarily N_2). As a result, the temporal and spatial variations of O/N_2 play an important role in the changes of plasma density in the F-region. The primary purpose of the present work is to study the longitudinal O/N_2 variation and search for tidal signatures in the O/N_2 ratio. After a brief description about the dataset in Section 2, we present the longitudinal O/N_2 structure and identify their possible origin in Section 3.

2. Data

[5] The NASA's Thermosphere, Ionosphere, and Mesosphere, Energetics and Dynamics (TIMED) spacecraft orbits at 630 km altitude with an inclination of 74.1° [*Christensen et al.*, 2003]. An instrument on board the TIMED is the Global Ultraviolet Imager (GUVI), which measures the brightness of the far ultraviolet (FUV) airglow in five bands: 121.6 nm, 130.4 nm, 135.6 nm, 141.0–152.8 nm, and 167.2–181.2 nm. It returns the images of the five "colors" with global coverage, which can be used to monitor the composition, temperature, large-scale wave structure, and auroral processes in the upper atmosphere. The column abundance of thermospheric atomic oxygen relative to molecular nitrogen is derived from the simultaneous measurements of disk-viewing dayglow of OI (135.6 nm) and N_2 Lyman-Birge-Hopfield (LBH) [*Strickland et al.*, 2004]. The derived O/N_2 is the ratio of height-integrated O density to the height-integrated N_2 density above a reference level near the bottom of the photoelectron-excited dayglow layer (a variable altitude of approximate 140 km, above which the height-integrated density of N_2 is 10^{17} cm^{-2}). Thermospheric O/N_2 for this investigation is level 3 data obtained from the Johns Hopkins University Applied Physics Laboratory. We used the

[1]Beijing National Observatory of Space Environment, Institute of Geology and Geophysics, Chinese Academy of Sciences, Beijing, China.
[2]Graduate University, Chinese Academy of Sciences, Beijing, China.
[3]Aerospace Engineering Sciences, University of Colorado at Boulder, Boulder, Colorado, USA.

0094-8276/10/2010GL045105

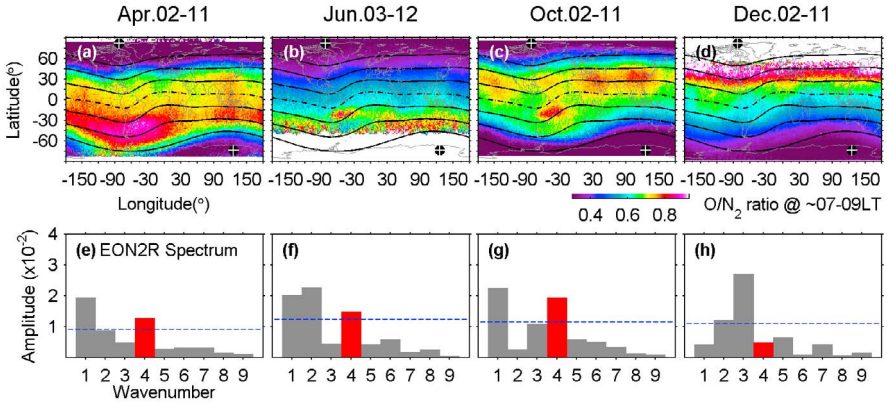

Figure 1. (a–d) Global maps of GUVI-measured O/N_2 ratio at 07–09 LT for the four seasons, and (e–h) the corresponding spectra of EON2R for Figures 1a–1d. In Figures 1–1d, white crosses on black dots stand for the geomagnetic poles; solid and dashed lines show contours of geomagnetic latitudes from 60°N to 60°S with an interval of 20°. In Figures 1e–1h, the dashed lines denote the 95% confidence level. Note that the TIMED satellite precesses at a rate of about 3° per day; accordingly the GUVI measurement always covers 10–12 LT sector at equinoxes but 16–18 LT at solstices. In order to examine the seasonal variation at same local time, we select four date windows centering at the days shifting about 15 days away from the exact equinoxes and solstices respectively.

measurements within the period from day of year (DOY) 008, 2002 to DoY 307, 2007.

3. Results and Conclusions

[6] Figures 1a–1d show the global maps of GUVI-measured O/N_2 in four 10-day-wide windows around the equinoxes and solstices. In each date window, the 5 years of measurements collected during 07-09 LT under geomagnetically quiet condition are binned, and the median is computed for each grid with a resolution of 1.765° longitude by 1.765° latitude. The quiet condition is characterized by AE6 index < 300nT [*Werner and Prölss*, 1997] and Estimated Hemispheric Power < 30GW [e.g., *Emery et al.*, 2008]. The most distinct feature in Figures 1a–1d is the asymmetry between the Northern and Southern Hemispheres, i.e., the O/N_2 ratio is generally lower in the Hemisphere where the subsolar point locates at (the Southern Hemisphere in October and December and the Northern Hemisphere in April and June). This feature could be attributed to the transequatorial neutral wind driven by the latitudinal gradient of solar irradiance heating [*Roble et al.*, 1977]. Meanwhile, the O/N_2 ratio in Figures 1a–1d exhibit prominent longitudinal variations. In the northern and Southern Hemispheres, the O/N_2 ratio is generally lower in the longitudinal sectors near the local geomagnetic pole (90°W in the Northern Hemisphere and 120°E in the Southern Hemisphere) than that in longitudinal sectors away from the pole. This longitudinal structure might have a contribution to the Weddell Sea Anomaly [*He et al.*, 2009] and could arise from the fact that the north and south geomagnetic poles locate at different longitudes [e.g., *Rishbeth and Müller-Wodarg*, 1999; *Lei et al.*, 2010]. Furthermore, a striking four-peaked longitudinal structure is clearly visible around September Equinox (Figure 1c). Between 20°S and 40°N geomagnetic latitudes, the O/N_2 ratio peaks distinctly around 150°W, 50°W, 30°E and 120°E. In other seasons the zonal fluctuation can also be observed around the geomagnetic equator, although four-peaked structure is not clearly seen as that around September Equinox.

[7] To compare each component in the zonal O/N_2 fluctuation, a Fourier analysis is performed for the Equatorial O/N_2 Ratio (EON2R). The EON2R, the averaged O/N_2 within ±20° geomagnetic latitudes, is calculated by the following equation with a longitudinal interval of 7.05°:

$$EON2R(Lon) = \frac{1}{Lat_N - Lat_S}\int_{Lat_S}^{Lat_N} O/N_2(Lon, Lat)dLat$$

The Fourier amplitude spectra of the EON2R of Figures 1a–1d are exhibited in Figures 1e–1h, respectively. Generally, the significant components are wavenumber-1, 2, 3, and 4. The WN4 component presents a seasonal variation. It is strong around September Equinox, less strong around June Solstice and March Equinox, and weak around December Solstice, which is consistent with the seasonal variation of the WN4 signatures in total electron content (TEC), vertical plasma drifts, temperature, and zonal wind [*Kil et al.*, 2008; *Oberheide and Forbes*, 2008b; *Wan et al.*, 2008; *Ren et al.*, 2009]. It is broadly believed that the DE3 tide excited in the tropical troposphere is the major contributor to the observed WN4 in various ionosphere-thermosphere properties [*Hagan et al.*, 2007; *Wan et al.*, 2008]. The DE3 mode is the most dominant component in all nonmigrating tidal modes for most of the year, but it experiences a considerable intraannual variation [e.g., *Oberheide et al.*, 2006] and sometimes can be met or exceeded by the diurnal eastward-propagating mode with wavenumber-2 (DE2), [*Häusler et al.*, 2007; *Pedatella et al.*, 2008; *Forbes et al.*, 2008, 2009; *Häusler and Lühr*, 2009]. Although the details of DE3 mode may vary with altitude, solar activity level or measuring method, there is a consensus that the DE3 mode maximizes during July–September, and it is dominant mainly during boreal summer and autumn but in an inferior position during boreal winter compared with the DE2 mode. When the DE2 dominates over the DE3, a zonal wavenumber-3 (WN3) structure could be observed in a fixed local time frame [*Oberheide and Forbes*, 2008a]. Such seasonal transition from WN4 to WN3 was observed in the zonal fluctuations of in-situ electron densities [*Pedatella et al.*,

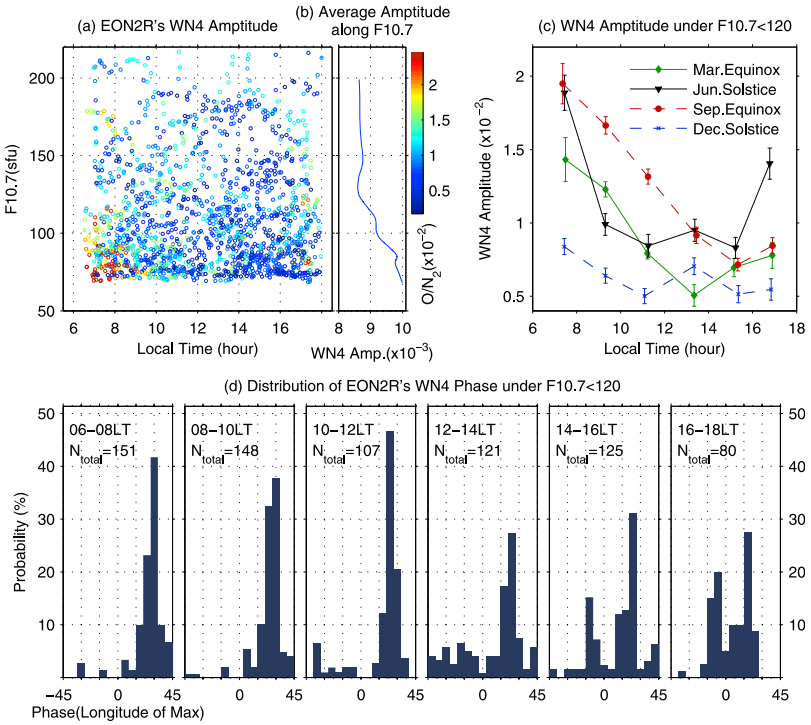

Figure 2. (a) F10.7 and LT distribution of WN4 amplitude of daily EON2R spectrum during 2002–2007. (b) Average of the daily WN4 amplitude along F10.7. (c) Seasonal variations of daytime WN4 amplitude under F10.7<120. Errorbars indicate the standard deviations (the errorbars are reduced to their 20% for better visibility). (d) WN4 phase distribution of the daily EON2R spectrum for different LT bands under F10.7<120. Because of the nature of four complete periods for WN4 from −180° to 180°, we showed the phase values in the range of −45°–45°. The components below 90% confident level are not shown in this plot.

2008], nitric oxide densities [*Oberheide and Forbes*, 2008a], and other ionospheric and thermospheric properties. In Figure 1h, the amplitude of WN4 component declines around December Solstice while the WN3 component enhances, compared with that in the other seasons.

[8] GUVI's measurements in a 9-day-wide sliding window from DoY 008, 2002 to DoY 307, 2007 are binned to construct global O/N_2 maps similar as those in Figures 1a–1d. In total, 1749 maps are constructed. The EON2R and its Fourier spectra for each map are calculated. The WN4 amplitudes of the series of EON2R spectrum are showed in Figure 2a as a function of LT and the 9 days mean of 10.7 cm solar radio flux (F10.7, in unit of sfu, 1sfu=10^{-22} W·m^{-2}·Hz^{-1}). Figure 2b shows the average of the WN4 amplitudes along F10.7. It is clear from Figures 2a and 2b that the WN4 amplitude is generally smaller at higher F10.7 level, which is consistent with the F10.7 dependence of DE3 mode [e.g., *Oberheide et al.*, 2009], possibly resulting from the enhanced tidal dissipation at higher solar activity caused by the temperature dependence (proportional to $T^{2/3}$) of molecular thermal conductivity [*Oberheide et al.*, 2009]. Another notable feature in Figure 2a is the LT dependence. The LT dependence is studied by binning the WN4 amplitudes under F10.7<120 within six LT bands and four seasons (91 days around equinox or solstice). As shown in Figure 2c, the WN4 amplitude is most significant at 06–08 LT band during June Solstice and September Equinox; it declines during the following hours and turns to growth before 18 LT.

[9] If the DE3 tide dominates the WN4 pattern in O/N_2, the pattern should be propagating eastward with a speed of about 90° per day observed in the LT-frame as the DE3-induced WN4 patterns in some other properties [e.g., *Wan et al.*, 2008; *Häusler and Lühr*, 2009]. The WN4 phase distributions, for the six LT bands, of the series of EON2R spectrum are present in Figure 2d. The WN4 component peaks most probably between 21–33°E from 06–08 to 14–16 LT, and the longitude of maximum probability does not shift eastward with local time. Note that the lack of local time shift is not masked by the seasonal variation. When the data were binned for each season, the feature of local time shift is still not found (not shown). Thus, it suggests the WN4 pattern in O/N_2 is not modulated directly by the DE3 tide in most of the daytime. Of all tide components contributing potentially to WN4 pattern, the stationary planetary with wavenumber-4 (sPW4) is the only stationary one. However, the sPW4 mode is significantly smaller than the DE3 mode [e.g., *Häusler and Lühr*, 2009; *Hagan et al.*, 2009] and it has not been reported to be mainly responsible for any WN4 signatures. To satisfy the observational constraints, we speculate that the WN4 pattern in O/N_2 might be excited by the DE3 tide at an earlier time, and then persists in local time.

[10] GUVI O/N_2 ratio is derived theoretically from the brightness ratio of photoelectron-impact-excited OI 135.6nm emission to N_2 LBH emission. In fact, the radiative recombination of oxygen ions and electrons will also produce 135.6nm emissions which are proportional to the product of the number densities of oxygen ion (N_{O+}) and electron (N_e), approximately equal to N_e^2 in the F-region. The remaining question is whether the radiative recombination could produce such a change that the WN4 fluctuation in the derived

O/N_2 is a signature of the fluctuation in N_e. If the WN4 in N_e is the main contributor to the fluctuation in the derived O/N_2, the O/N_2 ratio should peak at the N_e maximum. However, between 45°W and 45°E the WN4 fluctuation of N_e peaks at 35–30°W at 06 LT and shifts gradually to about 0–10°E before 18 LT with a diurnal maximal amplitude in the afternoon [*Wan et al.*, 2008], which are not consistent with those of the longitudinal structures in derived O/N_2 that peaks most probably at 21–33°E in the most daytime with the early diurnal maximal amplitude in the morning (Figures 2c and 2d). Actually, the radiative recombination emission contributes a small fraction to the height integration of 135.6nm emissions [cf. *Strickland et al.*, 2004; *Christensen et al.*, 2003]. Thus, the derived O/N_2 fluctuation should not be a direct measurement of the WN4 in N_e.

[11] One way to induce a tidal O/N_2 variation in the upper thermosphere is the fluctuation in temperature. In an equilibrium thermosphere, individual compositions distribute in static diffusion according to their own scale heights. At fixed altitudes, heavy compositions with smaller scale heights are affected more by temperature than light compositions. Then, thermal expansion would reduce the column abundance ratio of a light composition to a weighty composition for fixed altitudes. However, on a fixed pressure level the thermal expansion cannot change the O/N_2 ratio [*Rishbeth and Müller-Wodarg*, 1999]. GUVI O/N_2 is referenced to a fixed column density of N_2 (close to a fixed pressure level rather than a fixed altitude) and consequently is not sensitive to thermal changes combined with static diffusion [*Strickland et al.*, 2004]. The dynamical process provides another possible source. The WN4 fluctuation is also observed in thermospheric zonal wind [e.g., *Talaat and Lieberman*, 2010]. The uneven zonal winds could imply a divergence or convergence of the horizontal winds, which would be accompanied by upward or downward winds. Although there is no direct observation, the DE3 tidal vertical wind was predicted by *Oberheide and Forbes* [2008b] and *Oberheide et al.* [2009], using Hough Mode Extension analysis of horizontal wind and temperature measurements from the TIMED and CHAMP. The O/N_2 ratio could be decreased (increased) by upwelling (downwelling) motion [*Rishbeth and Müller-Wodarg*, 1999; *Lei et al.*, 2010]. Thus, more knowledge about DE3 tidal vertical wind can help to understanding the behaviors of the WN4 in O/N_2.

[12] In conclusion, the longitudinal fluctuation of equatorial O/N_2 ratio contains a considerable WN4 component. The WN4 component is strong during boreal summer and autumn. In boreal winter, the WN4 component declines, accompanied with an enhanced WN3 component. The WN4 component exhibits a clear F10.7 dependence that it is generally stronger at lower F10.7 level. The seasonal variation and F10.7 dependence are consistent with those of the DE3 tide mode, indicating a potential connection with the DE3 tide mode. However, the WN4 fluctuation in O/N_2 maximizes in the morning sector and its phase is almost stationary during the daytime. To satisfy the observations, we speculate that the daytime WN4 structure in O/N_2 is persistence from a pattern excited at an earlier time. Some physical mechanisms were examined to explain this structure, but all mechanisms had issues. Because the ionization density in the F-region is sensitive to the variations in O/N_2 ratio, the longitudinal WN4 structure in O/N_2 could contribute to the longitudinal distribution of the ionospheric plasma.

[13] **Acknowledgments.** The authors thank the referees for their comments to improve greatly the manuscript. M. He thanks Z. Ren for his useful discussions. This research was supported by National Natural Science Foundation of China (40725014) and National Important Basic Research Project (2006CB806306) as well as Project supported by the Specialized Research Fund for State Key Laboratories. This study made use of the GUVI data from the Johns Hopkins University Applied Physics Laboratory. We thank PI Dr. Andrew Christensen for suggestions in the usage of GUVI data.

References

Christensen, A. B., et al. (2003), Initial observations with the Global Ultraviolet Imager (GUVI) in the NASA TIMED satellite mission, *J. Geophys. Res.*, *108*(A12), 1451, doi:10.1029/2003JA009918.

Emery, B. A., V. Coumans, D. S. Evans, G. A. Germany, M. S. Greer, E. Holeman, K. Kadinsky-Cade, F. J. Rich, and W. Xu (2008), Seasonal, Kp, solar wind, and solar flux variations in long-term single-pass satellite estimates of electron and ion auroral hemispheric power, *J. Geophys. Res.*, *113*, A06311, doi:10.1029/2007JA012866.

England, S. L., T. J. Immel, E. Sagawa, S. B. Henderson, M. E. Hagan, S. B. Mende, H. U. Frey, C. M. Swenson, and L. J. Paxton (2006), Effect of atmospheric tides on the morphology of the quiet time, post-sunset equatorial ionospheric anomaly, *J. Geophys. Res.*, *111*, A10S19, doi:10.1029/2006JA011795.

Forbes, J. M., X. Zhang, S. Palo, J. Russell, C. J. Mertens, and M. Mlynczak (2008), Tidal variability in the ionospheric dynamo region, *J. Geophys. Res.*, *113*, A02310, doi:10.1029/2007JA012737.

Forbes, J. M., S. L. Bruinsma, X. Zhang, and J. Oberheide (2009), Surface-exosphere coupling due to thermal tides, *Geophys. Res. Lett.*, *36*, L15812, doi:10.1029/2009GL038748.

Hagan, M. E., and J. M. Forbes (2002), Migrating and nonmigrating diurnal tides in the middle and upper atmosphere excited by tropospheric latent heat release, *J. Geophys. Res.*, *107*(D24), 4754, doi:10.1029/2001JD001236.

Hagan, M. E., A. Maute, R. G. Roble, A. D. Richmond, T. J. Immel, and S. L. England (2007), Connections between deep tropical clouds and the Earth's ionosphere, *Geophys. Res. Lett.*, *34*, L20109, doi:10.1029/2007GL030142.

Hagan, M. E., A. Maute, and R. G. Roble (2009), Tropospheric tidal effects on the middle and upper atmosphere, *J. Geophys. Res.*, *114*, A01302, doi:10.1029/2008JA013637.

Häusler, K., and H. Lühr (2009), Nonmigrating tidal signals in the upper thermospheric zonal wind at equatorial latitudes as observed by CHAMP, *Ann. Geophys.*, *27*, 2643–2652, doi:10.5194/angeo-27-2643-2009.

Häusler, K., H. Lühr, S. Rentz, and W. Köhler (2007), A statistical analysis of longitudinal dependences of upper thermospheric zonal winds at dip equator latitudes derived from CHAMP, *J. Atmos. Sol. Terr. Phys.*, *69*, 1419–1430, doi:10.1016/j.jastp.2007.04.004.

He, M., L. Liu, W. Wan, B. Ning, B. Zhao, J. Wen, X. Yue, and H. Le (2009), A study of the Weddell Sea anomaly observed by FORMOSAT-3/COSMIC, *J. Geophys. Res.*, *114*, A12309, doi:10.1029/2009JA014175.

Huang, C.-S., F. J. Rich, O. de La Beaujardiere, and R. A. Heelis (2010), Longitudinal and seasonal variations of the equatorial ionospheric ion density and eastward drift velocity in the dusk sector, *J. Geophys. Res.*, *115*, A02305, doi:10.1029/2009JA014503.

Immel, T. J., E. Sagawa, S. L. England, S. B. Henderson, M. E. Hagan, S. B. Mende, H. U. Frey, C. M. Swenson, and L. J. Paxton (2006), Control of equatorial ionospheric morphology by atmospheric tides, *Geophys. Res. Lett.*, *33*, L15108, doi:10.1029/2006GL026161.

Kil, H., E. R. Talaat, S.-J. Oh, L. J. Paxton, S. L. England, and S.-J. Su (2008), Wave structures of the plasma density and vertical E×B drift in low-latitude F region, *J. Geophys. Res.*, *113*, A09312, doi:10.1029/2008JA013106.

Lei, J., J. P. Thayer, A. G. Burns, G. Lu, and Y. Deng (2010), Wind and temperature effects on thermosphere mass density response to the November 2004 geomagnetic storm, *J. Geophys. Res.*, *115*, A05303, doi:10.1029/2009JA014754.

Liu, H., M. Yamamoto, and H. Lühr (2009a), Wave-4 pattern of the equatorial mass density anomaly: A thermospheric signature of tropical deep convection, *Geophys. Res. Lett.*, *36*, L18104, doi:10.1029/2009GL039865.

Liu, L., B. Zhao, W. Wan, B. Ning, M.-L. Zhang, and M. He (2009b), Seasonal variations of the ionospheric electron densities retrieved from Constellation Observing System for Meteorology, Ionosphere, and Climate mission radio occultation measurements, *J. Geophys. Res.*, *114*, A02302, doi:10.1029/2008JA013819.

Oberheide, J., and J. M. Forbes (2008a), Thermospheric nitric oxide variability induced by nonmigrating tides, *Geophys. Res. Lett.*, *35*, L16814, doi:10.1029/2008GL034825.

Oberheide, J., and J. M. Forbes (2008b), Tidal propagation of deep tropical cloud signatures into the thermosphere from TIMED observations, *Geophys. Res. Lett.*, *35*, L04816, doi:10.1029/2007GL032397.

Oberheide, J., M. E. Hagan, and R. G. Roble (2003), Tidal signatures and aliasing in temperature data from slowly precessing satellites, *J. Geophys. Res.*, *108*(A2), 1055, doi:10.1029/2002JA009585.

Oberheide, J., Q. Wu, T. L. Killeen, M. E. Hagan, and R. G. Roble (2006), Diurnal nonmigrating tides from TIMED Doppler Interferometer wind data: Monthly climatologies and seasonal variations, *J. Geophys. Res.*, *111*, A10S03, doi:10.1029/2005JA011491.

Oberheide, J., J. M. Forbes, K. Häusler, Q. Wu, and S. L. Bruinsma (2009), Tropospheric tides from 80 to 400 km: Propagation, interannual variability, and solar cycle effects, *J. Geophys. Res.*, *114*, D00I05, doi:10.1029/2009JD012388.

Pedatella, N. M., J. M. Forbes, and J. Oberheide (2008), Intra-annual variability of the low-latitude ionosphere due to nonmigrating tides, *Geophys. Res. Lett.*, *35*, L18104, doi:10.1029/2008GL035332.

Ren, Z., W. Wan, L. Liu, B. Zhao, Y. Wei, X. Yue, and R. A. Heelis (2008), Longitudinal variations of electron temperature and total ion density in the sunset equatorial topside ionosphere, *Geophys. Res. Lett.*, *35*, L05108, doi:10.1029/2007GL032998.

Ren, Z., W. Wan, L. Liu, and J. Xiong (2009), Intra-annual variation of wave number 4 structure of vertical E×B drifts in the equatorial ionosphere seen from ROCSAT-1, *J. Geophys. Res.*, *114*, A05308, doi:10.1029/2009JA014060.

Rishbeth, H., and I. C. F. Müller-Wodarg (1999), Vertical circulation and thermospheric composition: A modelling study, *Ann. Geophys.*, *17*, 794–805, doi:10.1007/s00585-999-0794-x.

Roble, R. G., R. E. Dickinson, and E. C. Ridley (1977), Seasonal and solar cycle variations of the zonal mean circulation in the thermosphere, *J. Geophys. Res.*, *82*, 5493–5504, doi:10.1029/JA082i035p05493.

Strickland, D. J., R. R. Meier, R. L. Walterscheid, J. D. Craven, A. B. Christensen, L. J. Paxton, D. Morrison, and G. Crowley (2004), Quiet-time seasonal behavior of the thermosphere seen in the far ultraviolet dayglow, *J. Geophys. Res.*, *109*, A01302, doi:10.1029/2003JA010220.

Talaat, E. R., and R. S. Lieberman (2010), Direct observations of non-migrating diurnal tides in the equatorial thermosphere, *Geophys. Res. Lett.*, *37*, L04803, doi:10.1029/2009GL041845.

Wan, W., L. Liu, X. Pi, M.-L. Zhang, B. Ning, J. Xiong, and F. Ding (2008), Wavenumber-4 patterns of the total electron content over the low latitude ionosphere, *Geophys. Res. Lett.*, *35*, L12104, doi:10.1029/2008GL033755.

Werner, S., and G. W. Prölss (1997), The position of the ionospheric trough as a function of local time and magnetic activity, *Adv. Space Res.*, *20*(9), 1717–1722, doi:10.1016/S0273-1177(97)00578-4.

M. He, L. Liu, W. Wan, and B. Zhao, Beijing National Observatory of Space Environment, Institute of Geology and Geophysics, Chinese Academy of Sciences, Beijing, 100029, China. (liul@mail.iggcas.ac.cn)

J. Lei, Aerospace Engineering Sciences, University of Colorado at Boulder, Boulder, CO 80309, USA.